Frequency domain modeling of nonlinear end stop behavior in Tuned Mass Damper systems under single- and multi-harmonic excitations

van Til, J.; Alijani, F.; Voormeeren, S. N.; Lacarbonara, W.

DOI
10.1016/j.jsv.2018.09.015

Publication date
2019

Document Version
Accepted author manuscript

Published in
Journal of Sound and Vibration

Citation (APA)
van Til, J., Alijani, F., Voormeeren, S. N., & Lacarbonara, W. (2019). Frequency domain modeling of nonlinear end stop behavior in Tuned Mass Damper systems under single- and multi-harmonic excitations. *Journal of Sound and Vibration*, *438*, 139-152. https://doi.org/10.1016/j.jsv.2018.09.015

Frequency domain modeling of nonlinear end stop behavior in Tuned Mass Damper systems under single- and multi-harmonic excitations

J. van Til[a], F. Alijani[a,*], S. N. Voormeeren[b], W. Lacarbonara[c]

[a] *Faculty of Mechanical, Maritime and Materials Engineering, Delft University of Technology, Mekelweg 2, 2628CD Delft, The Netherlands*
[b] *Siemens Gamesa Renewable Energy B.V., Offshore Engineering, Prinses Beatrixlaan 800, 2595 BN Den Haag, The Netherlands*
[c] *Department of Structural and Geotechnical Engineering, Sapienza University of Rome, Via Eudossiana 18, 00184 Rome, Italy*

Abstract

Nonsmooth dynamics of a Tuned Mass Damper system with lateral stops are studied using an alternating frequency/time harmonic balancing (AFT-HB) method. To this end, an extremely stiff end stop nonlinearity is considered. The application range of AFT-HB is investigated by including up to 250 harmonics in the external force, as well as in the motion description. Numerical simulations are performed by making use of a Newmark time integration algorithm for numerical verification of the results. The results for single harmonic excitations are further verified with an existing pseudo-arclength path-following tool. Two excitation scenarios are considered: single harmonic- and a wide-spectrum excitation with uniform distribution and random phase correlation between the harmonics. The AFT-HB algorithm is found to

*Corresponding author: F. Alijani, Department of Precision and Microsystems Engineering, 3mE, Mekelweg 2, 2628 CD, Delft, The Netherlands.
Email: f.alijani@tudelft.nl

accurately reproduce the time integration results, for all considered cases. Finally, insights are gained into the differences between the system responses to single- and multi-harmonic excitations.
Keywords: Nonlinear end stop, Tuned Mass Damper, Harmonic balance, Multi harmonic.

1. Introduction

Tuned mass dampers (TMDs) are passive vibration absorbers that are installed, for instance, in tall constructions, road vehicles, wind turbines and power transmissions, with the purpose of limiting the adverse effects of resonant excitations such as wind, waves (eg, for offshore wind turbines), and seismic excitations [1–4]. While optimal design theory for linear TMDs has been thoroughly investigated, there are very intense ongoing research efforts towards the development of nonlinear TMDs [5–12]. Due to the energy transfer between the structure and the TMD, the absorber experiences large displacements. Hence, an end stop effect can occur either as a direct result of the limited stroke of the device, or built in intentionally due to operational constraints.

For TMDs with a solid oscillating mass, suitable end stops are sometimes implemented in order to prevent the TMD from colliding with the structure walls. Modeling the dynamics of end stops is essential, since end stop collisions disturb the designed phase difference between the TMD and structure motions, which is central to the TMD performance. Moreover, multi-frequency excitations can further complicate the problem.

Minimizing the computational cost of simulation of this stiff nonlinear behavior is crucial for optimizing the design process. Frequency domain

techniques offer alternatives to slow nonlinear time integration schemes. Although several different frequency domain methods exist for nonlinear dynamics, the options reduce drastically when the problem is nonsmooth or contains many harmonics in the excitation. Closed form solutions such as perturbation techniques [13] require analytic approximations of the non-smooth functions, making the end stop model less realistic. While certain path-following methods [14] are capable of implementing stiffness discontinuities [15], these methods cannot deal with multi-harmonic external loads, unless certain restrictions are placed on the form of the excitation or the period of the response.

The Alternating Frequency / Time (AFT-HB) method has been applied to several classes of nonsmooth problems. In the method, iteration is performed on the vector of harmonic components in the solution. Since the nonlinear forces (as well as their derivatives) are evaluated in the time domain, this nonlinear force can be of nonsmooth nature, and an arbitrary number of harmonic components can theoretically be included in the excitation (as well as the solution). Being able to handle nonsmooth systems carrying many harmonic components, the AFT-HB method has the potential to tackle the problem in question, in contrast to the previously listed methods (path-following as well as closed form solutions).

The AFT-HB technique was implemented successfully to study one- and two-degree-of-freedom (dof) systems with bilinear hysteretic nonlinearity, under single harmonic excitations [16]. The same method was applied to a bearing-rotor problem with contact dynamics, where frequency responses were successfully obtained using the AFT-HB algorithm [17]. Piecewise nonlinearities have also been tackled by a similar approach [18, 19]. The response of dry-

damped one- and two-dof systems to dynamic excitations containing a few harmonic components was studied [19], after which the results showed a good agreement with results obtained by time integration. However, it is unclear how AFT-HB performs in case of excitations containing hundreds of harmonic components, with a strong nonlinearity as an end stop.

The above state of the art leads to the motivation for further investigating the AFT-HB method in this work. In this respect, AFT-HB has been applied to single- and two-dof systems with end stop nonlinearity. The results of the numeric investigations are discussed. The single-dof system is treated first, since this system allows one to study and verify the end stop behavior without any interaction between mechanical bodies. Next, a two-dof mechanical system is presented to represent the main structure with an attached TMD. To crosscheck the results obtained by the AFT-HB method, a Newmark time integration scheme is implemented and applied to obtain reference results. The AFT-HB algorithm is shown to deal well with both the single-dof and two-dof systems, under single- as well as multi-harmonic external forces. The results for single harmonic excitations are further corroborated by the results of a pseudo-arclength (PSA) path-following tool [15].

2. Equations of Motion

An N-dof nonlinear system describing a displacement $\mathbf{u} \in R^{\mathrm{N}}$ with $\mathrm{N} \geq 1$ subject to an external forcing function $\mathbf{f}^{\mathrm{ext}}(t)$ can be described as

$$\mathbf{M}\ddot{\mathbf{u}} + \mathbf{C}\dot{\mathbf{u}} + \mathbf{K}\mathbf{u} + \mathbf{f}^{\mathrm{NL}} = \mathbf{f}^{\mathrm{ext}}. \tag{1}$$

where $\mathbf{f}^{\mathrm{NL}}$ is the nonlinear restoring force, $\mathbf{M}$, $\mathbf{K}$ and $\mathbf{C}$ are the mass, stiffness, and damping matrices, respectively.

A two-dof damped structure is the simplest reduced-order model of any structure, damped by a TMD, as shown in Fig. 1 where the end stop mechanism is also sketched.

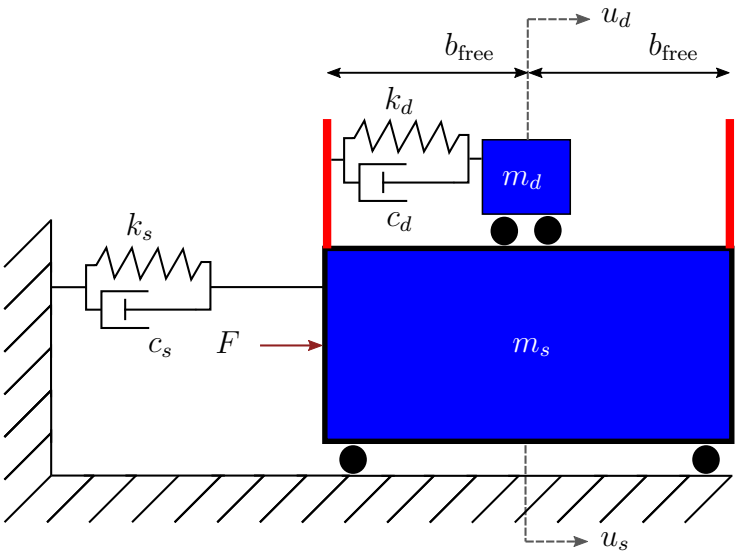

Figure 1: Two-dof oscillator with end stops. The end stops are illustrated by the two vertical barriers located on top of the structure body, limiting the motion of the TMD.

The system consists of a rigid body representing the damped structure with mass m_s, connected to ground via a linear spring of constant k_s and dashpot of viscosity c_s. The structure is subjected to an external force F. The tuned mass is, in turn, connected to the structure, via a linear spring of constant k_d and a dashpot of viscosity c_d, and its free motion relative to the main structure is limited by the end stop to b_{free}. The equations of motion for

this system under external force $\mathbf{f}^{\text{ext}} = [0 \quad F]^{\text{T}}$, whose displacement vector is $\mathbf{u} = [u_d \quad u_s]^{\text{T}}$, read:

$$\begin{aligned} \mathbf{M} &= \begin{bmatrix} m_d & 0 \\ 0 & m_s \end{bmatrix}, \\ \mathbf{C} &= \begin{bmatrix} c_d & -c_d \\ -c_d & c_s + c_d \end{bmatrix}, \\ \mathbf{K} &= \begin{bmatrix} k_d & -k_d \\ -k_d & k_s + k_d \end{bmatrix}. \end{aligned} \tag{2}$$

With $u = u_d - u_s$ representing the displacement of the damper relative to the structure, the nonlinear restoring force is defined as follows:

$$\begin{aligned} \mathbf{f}^{\text{NL}} &= \begin{bmatrix} f^{\text{NL}}(u) \\ 0 \end{bmatrix}, \\ f^{\text{NL}}(u) &= \end{aligned} \tag{3}$$

$$\begin{cases} k_2 \left(|u| - b_{\text{free}} \right)^{3/2} \cdot \text{sign}\left(u\right) & |u| - b_{\text{free}} \geq 0 \\ 0 & |u| - b_{\text{free}} < 0 \end{cases},$$

where k_2 is the spring constant of the end stop. For the elastic end stop force f^{NL}, a Hertz contact model is here employed, in agreement with a variety of problems covering pounding between structures [20–22]. The $\frac{3}{2}$ - power law in terms of the impact penetration depth $|u| - b_{\text{free}} > 0$ holds for the following configurations of colliding bodies: sphere-sphere, sphere-plane, and cylinder-cylinder (with misaligned axes law in terms of). When

the colliding bodies are arbitrary, it is conventional to use the sphere-sphere approximation. Jankowski's model (based on Hertzian contact) was tested through comparisons between numerical studies of structure impacts, and was shown to be in very good agreement with experimental results, thus justifying its usage its usage in the present work [20].
The derivatives of the end stop force w. r. t. the structure and TMD motions become, respectively:

$$\frac{\partial f^{\mathrm{NL}}}{\partial u_s} = \begin{cases} -\frac{3}{2}k_2\left(|u| - b_{\mathrm{free}}\right)^{1/2} & |u| - b_{\mathrm{free}} \geq 0 \\ 0 & |u| - b_{\mathrm{free}} < 0 \end{cases}, \tag{4}$$

$$\frac{\partial f^{\mathrm{NL}}}{\partial u_d} = \begin{cases} \frac{3}{2}k_2\left(|u| - b_{\mathrm{free}}\right)^{1/2} & \text{as above.} \\ 0 \end{cases} \tag{5}$$

Realistically, an end stop would contain some damping, dissipating the kinetic energy of the tuned mass, in addition to the damper between the TMD and the structure. Thus, the net amount of damping would increase when the end stop is impacted by the TMD. This could deteriorate the TMD performance in two different ways. Firstly, exceeding the amount of damping in the design specification could limit the TMD motion too much to function effectively. Secondly, a higher net damping could alter the eigenfrequency of the TMD from the optimal value. For these reasons, an end stop ought to be designed fairly elastic. Therefore it was decided to use the extreme case of a purely elastic end stop throughout this work, where investigating (a range of) end stop damping is left as a recommendation.

For the sake of investigating solely the end stop behavior without interaction

between bodies, a schematic of an single-dof oscillator with end stops is shown in Fig. 2.

The corresponding equations of motion are given by

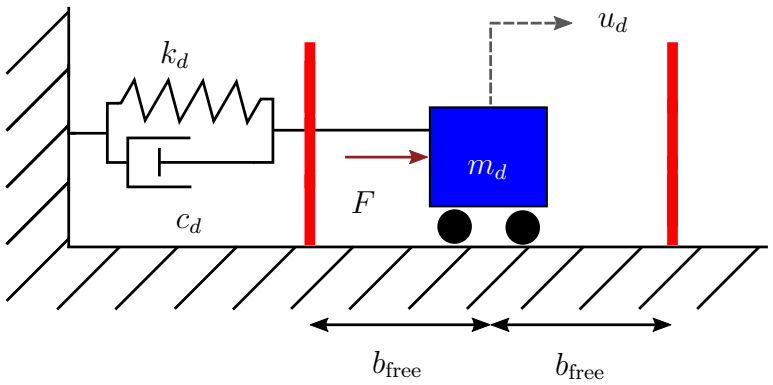

Figure 2: Single-dof oscillator with end stops, illustrated by the vertical barriers.

$$m_d\ddot{u}_d + c_d\dot{u}_d + k_d u_d + f^{\text{NL}}(u_d) = F, \tag{6}$$

$$f^{\text{NL}}(u_d) = \begin{cases} k_2 \,\text{sign}\,(u_d)\,|u_d - b_{\text{free}}|^{3/2} & \text{as above.} \\ 0 \end{cases} \tag{7}$$

3. Harmonic Balancing with Alternating Frequency/Time

The starting point of the harmonic balance method [19] is to express the displacement $\mathbf{u}$ (u in Eq. 6 and $\mathbf{u} = \begin{bmatrix} u_{\text{d}} & u_{\text{s}} \end{bmatrix}^T$ in Eq. 1) in a number of harmonics $k = 1, 2, \ldots K$, with corresponding amplitudes $\mathbf{a}_k$ and $\mathbf{b}_k$ thus yielding $\mathbf{u}_K(t)$:

$$\mathbf{u}_K(t) = \mathbf{a}_0 + \sum_{k=1}^{K} \left[\mathbf{a}_k \cos(\omega_k t) + \mathbf{b}_k \sin(\omega_k t)\right], \tag{8}$$

$$\dot{\mathbf{u}}_K(t) = \sum_{k=1}^{K} \left[\omega_k \left(-\mathbf{a}_k \sin(\omega_k t) + \mathbf{b}_k \cos(\omega_k t)\right)\right], \tag{9}$$

$$\ddot{\mathbf{u}}_K(t) = \sum_{k=1}^{K} \left[\omega_k^2 \left(-\mathbf{a}_k \cos(\omega_k t) - \mathbf{b}_k \sin(\omega_k t)\right)\right]. \tag{10}$$

The higher harmonics are expressed as integer multiples of the first harmonic ω_1, so $\omega_k = k\omega_1$. The external excitation may consist of an arbitrary number of frequencies ω_s with corresponding phases ϕ_s, yielding the following equation of motion cast in vector-valued form:

$$\mathbf{M}\ddot{\mathbf{u}} + \mathbf{C}\dot{\mathbf{u}} + \mathbf{K}\mathbf{u} + \mathbf{f}^{\mathrm{NL}}(\mathbf{u}) = \mathbf{F} = \sum_{s=1}^{S} \mathbf{p}_s \sin\left(k\omega_s t + \phi_s\right). \tag{11}$$

The phases ϕ_s can be separated from the sine function by adding cosines, doubling the number of harmonic terms and using the trigonometric identity:

$$\sin\left(k\omega_s t + \phi_s\right) = \cos\left(k\omega_s t\right) \sin\phi_s + \sin\left(k\omega_s t\right) \cos\phi_s. \tag{12}$$

For a system with N degrees of freedom, the goal is to obtain NK equations for the cosine contributions, NK for the sines, and N for the DC terms ($\mathbf{a}_0$), thus solving a total of $2NK + N$ unknowns: $\mathbf{a}_0$, $\mathbf{a}_k$ and $\mathbf{b}_k$. Following Eq. 12, the nonlinear force $\mathbf{f}^{\mathrm{NL}}$ can also be expressed as a sum of harmonics:

$$\mathbf{f}_K^{\mathrm{NL}}(t) = \mathbf{c}_0 + \sum_{k=1}^{K} \left[\mathbf{c}_k \cos(\omega_k t) + \mathbf{d}_k \sin(\omega_k t)\right]. \tag{13}$$

Hereby, another $2NK+N$ unknowns are introduced. The reverse relationship lies in the Fourier Transform [23]:

$$\mathbf{c}_0 = \frac{1}{2\pi}\int_0^{2\pi} \left(\mathbf{f}_K^{\mathrm{NL}}(t)\right) dt, \tag{14}$$

$$\mathbf{c}_k = \frac{1}{\pi}\int_0^{2\pi} \left(\mathbf{f}_K^{\mathrm{NL}}(t)\cos(\omega_k t)\right) dt, \tag{15}$$

$$\mathbf{d}_k = \frac{1}{\pi}\int_0^{2\pi} \left(\mathbf{f}_K^{\mathrm{NL}}(t)\sin(\omega_k t)\right) dt. \tag{16}$$

Finally, Eqns. 8 - 13 can be combined to balance the DC components and the harmonics corresponding to $\cos(\omega_k t)$ and $\sin(\omega_k t)$, respectively:

$$\mathbf{g}_{DC} = \mathbf{K}\mathbf{a}_0 + \mathbf{c}_0 = \mathbf{0}, \tag{17}$$

$$\mathbf{g}_{k,\cos} = -\left(\omega_k^2\mathbf{M} - \mathbf{K}\right)\mathbf{a}_k + \omega_k\mathbf{C}\mathbf{b}_k + \mathbf{c}_k - \mathbf{\Psi}_{k,\sin} = \mathbf{0}, \tag{18}$$

$$\mathbf{g}_{k,\sin} = -\omega_k\mathbf{C}\mathbf{a}_k - \left(\omega_k^2\mathbf{M} - \mathbf{K}\right)\mathbf{b}_k + \mathbf{d}_k - \mathbf{\Psi}_{k,\cos} = \mathbf{0}. \tag{19}$$

Here, $\mathbf{\Psi}_{k,\cos} = \mathbf{p}_k\cos\phi_k$ and $\mathbf{\Psi}_{k,\sin} = \mathbf{p}_k\sin\phi_k$. The extra unknowns $\mathbf{c}_0$, $\mathbf{c}^{(k)}$ and $\mathbf{d}^{(k)}$ are handled using the Alternating Frequency/Time method.

The AFT-HB method [19, 24] uses the Discrete Fourier Transform and its inverse in order to obtain the harmonic nonlinear force coefficients of the nonlinear force $\tilde{\mathbf{f}}^{\mathrm{NL}}$ (comprised of $\mathbf{c}_0$, $\mathbf{c}_k$ and $\mathbf{d}_k$) numerically, based on an initial estimate of the state vector $\tilde{\mathbf{q}} = [\mathbf{a}_0^T\ \mathbf{a}_1^T\ \mathbf{b}_1^T\ \mathbf{a}_2^T\ \mathbf{b}_2^T\ ..\ \mathbf{a}_K^T\ \mathbf{b}_K^T]^T$. From $\tilde{\mathbf{q}}$, $\mathbf{u}_K$ can be constructed via Eqns. 8 - 10. Inserting $\tilde{\mathbf{q}}$ and $\tilde{\mathbf{f}}^{\mathrm{NL}}$ in the harmonic balance equations (Eq. 17 -19) results in a residual $\mathbf{r}$, upon which a Newton-Raphson method is employed to iterate towards the solution. The complete algorithm of this method is shown in Fig. 3. Here, $\mathbf{J}$ is defined as the Jacobian (Eq. 32).

The process is started by an initial estimate of the response, with $\mathbf{a}_0^{(0)}$,

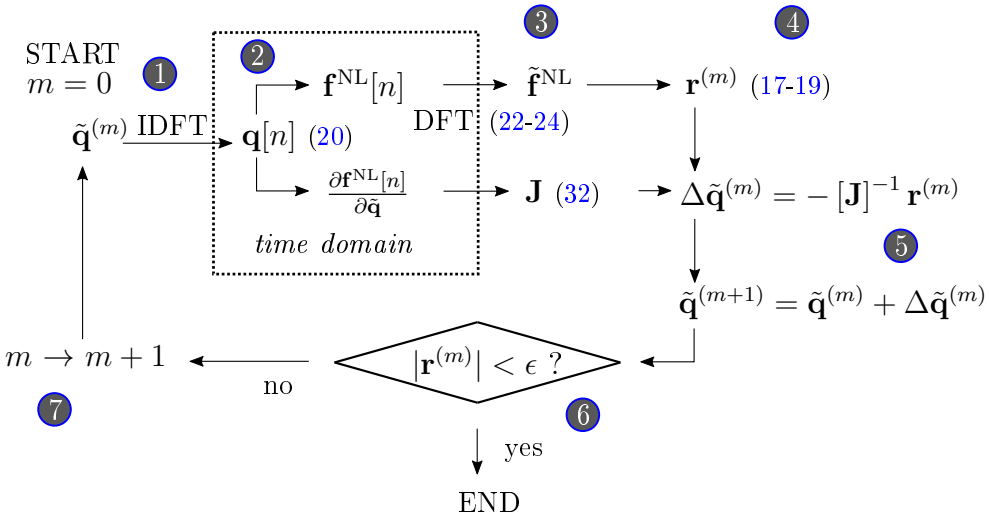

Figure 3: Harmonic Balance using the Alternating Frequency / Time method:

1. Construct a time series from state vector $\tilde{\mathbf{q}}^{(m)}$ through the Inverse Discrete Fourier Transform (IDFT).
2. Compute the nonlinear force, as well as its derivative, as time series.
3. Obtain the harmonic coefficients of the nonlinear force, as well as the Jacobian, through the Discrete Fourier Transform (DFT).
4. Compute the residual in the harmonic balance equations.
5. Compute and apply an update of the state vector.
6. Check whether convergence is reached. If not, proceed to step 7 and repeat steps 1-5.
7. Update the iteration number m.

$\mathbf{a}_k^{(0)}$ and $\mathbf{b}_k^{(0)}$. From this estimate, a discrete time series of the response can be constructed numerically, by applying the IDFT:

$$\mathbf{q}[n] = \mathbf{a}_0 + \sum_{k=1}^{K} \left[\mathbf{a}_k \cos\left(\frac{2\pi n k}{M}\right) + \mathbf{b}_k \sin\left(\frac{2\pi n k}{M}\right) \right]. \tag{20}$$

Next, a discrete time series of the nonlinear force can be computed as:

$$\mathbf{f}_K^{\mathrm{NL}}[n] = \mathbf{f}_K^{\mathrm{NL}}\left(\mathbf{q}[n]\right). \tag{21}$$

The integrals in Eqns. 14 - 16 are then evaluated numerically, using the DFT:

$$\mathbf{c}_0 = \frac{1}{M}\sum_{n=0}^{M-1}\left[\mathbf{f}_K^{\mathrm{NL}}[n]\right], \tag{22}$$

$$\mathbf{c}_k = \frac{2}{M}\sum_{n=0}^{M-1}\left[\mathbf{f}_K^{\mathrm{NL}}[n]\cos\left(\frac{2\pi nk}{M}\right)\right], \tag{23}$$

$$\mathbf{d}_k = \frac{2}{M}\sum_{n=0}^{M-1}\left[\mathbf{f}_K^{\mathrm{NL}}[n]\sin\left(\frac{2\pi nk}{M}\right)\right]. \tag{24}$$

Inserting the estimated response and the resulting nonlinear spectral coefficients in Eqns. 17-19 will yield the residual:

$$\mathbf{r}_{\mathrm{DC}} = \mathbf{g}_{\mathrm{DC}}(\mathbf{a}_0, \mathbf{c}_0), \tag{25}$$

$$\mathbf{r}_{k,\cos} = \mathbf{g}_{k,\cos}(\mathbf{a}_k, \mathbf{c}_k), \tag{26}$$

$$\mathbf{r}_{k,\sin} = \mathbf{g}_{k,\sin}(\mathbf{b}_k, \mathbf{d}_k). \tag{27}$$

The total residual $\mathbf{r}$, state coefficients $\tilde{\mathbf{q}}$, and nonlinear force coefficients $\tilde{\mathbf{f}}^{\mathrm{NL}}$ are assembled as follows:

$$\mathbf{r} = \underbrace{\begin{bmatrix} \mathbf{g}_{DC} \\ \mathbf{g}_{1,\cos} \\ \mathbf{g}_{1,\sin} \\ \mathbf{g}_{2,\cos} \\ \mathbf{g}_{2,\sin} \\ \vdots \\ \mathbf{g}_{K,\cos} \\ \mathbf{g}_{K,\sin} \end{bmatrix}}_{(28)} , \tilde{\mathbf{q}} = \underbrace{\begin{bmatrix} \mathbf{a}_0 \\ \mathbf{a}_1 \\ \mathbf{b}_1 \\ \mathbf{a}_2 \\ \mathbf{b}_2 \\ \vdots \\ \mathbf{a}_K \\ \mathbf{b}_K \end{bmatrix}}_{(29)} ; \quad \tilde{\mathbf{f}}^{\mathrm{NL}} = \underbrace{\begin{bmatrix} \mathbf{c}_0 \\ \mathbf{c}_1 \\ \mathbf{d}_1 \\ \mathbf{c}_2 \\ \mathbf{d}_2 \\ \vdots \\ \mathbf{c}_K \\ \mathbf{d}_K \end{bmatrix}}_{(30)} .$$

A Newton-Raphson scheme can be employed, to iterate towards the solution $\mathbf{q}$. The updates are found by inverting the Jacobian of the residual equation with respect to the states:

$$\tilde{\mathbf{q}}^{(m+1)} = \tilde{\mathbf{q}}^{(m)} - \left[\mathbf{J}^{(m)}\right]^{-1} \mathbf{r}^{(m)}, \tag{31}$$

in which

$$\mathbf{J} = \frac{\partial \mathbf{r}}{\partial \tilde{\mathbf{q}}} = \frac{\partial \mathbf{g}}{\partial \tilde{\mathbf{q}}} = \begin{bmatrix} \mathbf{K} & \mathbf{0} & \mathbf{0} & \cdots & \mathbf{0} \\ \mathbf{0} & \mathbf{\Phi}_1 & \mathbf{0} & \cdots & \mathbf{0} \\ \mathbf{0} & \mathbf{0} & \mathbf{\Phi}_2 & \cdots & \mathbf{0} \\ \vdots & \vdots & \vdots & \ddots & \vdots \\ \mathbf{0} & \mathbf{0} & \mathbf{0} & \cdots & \mathbf{\Phi}_K \end{bmatrix} + \frac{\partial \tilde{\mathbf{f}}^{\mathrm{NL}}}{\partial \tilde{\mathbf{q}}}, \tag{32}$$

$$\mathbf{\Phi}_k = \begin{bmatrix} -(\omega_k^2 \mathbf{M} - \mathbf{K}) & \omega_k \mathbf{C} \\ -\omega_k \mathbf{C} & (\omega_k^2 \mathbf{M} - \mathbf{K}) \end{bmatrix}. \tag{33}$$

The terms in $\mathbf{J}$ due to the nonlinear force, $\partial\tilde{\mathbf{f}}^{\mathrm{NL}}/\partial\tilde{\mathbf{q}}$, are found by taking the Jacobian of Eqns. 22-24 with respect to $\tilde{\mathbf{q}}$ as follows:

$$\frac{\partial \mathbf{c}_0}{\partial \tilde{\mathbf{q}}} = \frac{1}{M}\sum_{n=0}^{M-1}\left[\frac{\partial \mathbf{f}_K^{\mathrm{NL}}[n]}{\partial \tilde{\mathbf{q}}}\right], \tag{34}$$

$$\frac{\partial \mathbf{c}_k}{\partial \tilde{\mathbf{q}}} = \frac{2}{M}\sum_{n=0}^{M-1}\left[\frac{\partial \mathbf{f}_K^{\mathrm{NL}}[n]}{\partial \tilde{\mathbf{q}}}\cos\left(\frac{2\pi nk}{M}\right)\right], \tag{35}$$

$$\frac{\partial \mathbf{d}_k}{\partial \tilde{\mathbf{q}}} = \frac{2}{M}\sum_{n=0}^{M-1}\left[\frac{\partial \mathbf{f}_K^{\mathrm{NL}}[n]}{\partial \tilde{\mathbf{q}}}\sin\left(\frac{2\pi nk}{M}\right)\right], \tag{36}$$

$$\frac{\partial \mathbf{f}_K^{\mathrm{NL}}[n]}{\partial \tilde{\mathbf{q}}} = \frac{\partial \mathbf{f}_K^{\mathrm{NL}}[n]}{\partial \mathbf{q}[n]}\frac{\partial \mathbf{q}[n]}{\partial \tilde{\mathbf{q}}}, \tag{37}$$

where, from Eq. 20:

$$\frac{\partial \mathbf{q}[n]}{\partial \tilde{\mathbf{q}}_{i,j}} = \begin{cases} 1 & i = 1 \\ \cos\left(\frac{2\pi nj}{M}\right) & i = 2,4,6,...,2K \\ \sin\left(\frac{2\pi nj}{M}\right) & i = 3,5,7,...,2K+1 \end{cases}, \tag{38}$$

and for $\partial \mathbf{f}_K^{\mathrm{NL}}[n]/\partial \mathbf{q}[n]$ the closed-form derivatives $\partial \mathbf{f}^{\mathrm{NL}}/\partial \mathbf{u}$ are used, which were given in Eqns. 4 and 5.

4. Results and discussion

In order to demonstrate the broad application of the developed methodology, both the single-dof and two-dof systems with end stop nonlinearity subjected to single- and multi-harmonic excitations are studied.

4.1. Single-dof oscillator

The AFT-HB solution method is applied to the single-dof oscillator, illustrated in Fig. 2, and described by Eqns. 6 and 7. In order to show the magnitude of the nonlinear stiffness k_2 (Eq. 7) relative to the linear stiffness k_d (Eq. 6), the nondimensional form of Eq. 6 is provided. First, the following transformations are introduced:

$$t \rightarrow \tilde{t} = \omega_d t \tag{39}$$

$$\frac{\partial}{\partial t} \rightarrow \frac{\partial}{\partial \tilde{t}} = \frac{1}{\omega_d}\frac{\partial}{\partial t} \tag{40}$$

$$\frac{\partial^2}{\partial t^2} \rightarrow \frac{\partial^2}{\partial \tilde{t}^2} = \frac{1}{\omega_d^2}\frac{\partial^2}{\partial t^2} \tag{41}$$

$$u_d \rightarrow \tilde{u}_d = b_0 u_d, \tag{42}$$

where b_0 is a reference length, in this case chosen as $b_0 = b_{\text{free}}$, and ω_d is the natural frequency. Upon substituting the above transformations into Eq. 1, and dividing by $m_d \omega_d^2 b_{\text{free}}$, one obtains the following dimensionless equation of motion:

$$\ddot{\tilde{u}}_d + 2\zeta_d \dot{\tilde{u}}_d + \tilde{u}_d + \tilde{f}^{\text{NL}}(u_d) = \tilde{F}, \tag{43}$$

where:

$$\begin{aligned} \zeta_d &= \frac{c_d}{2m_d\omega_d}, \\ \tilde{F} &= \frac{F}{m_d\omega_d^2 b_{\text{free}}}, \\ \tilde{f}^{\text{NL}}(\tilde{u}_d) &= \end{aligned} \tag{44}$$

$$\begin{cases} \tilde{k}_2 \left(|\tilde{u}_d| - b_{\text{free}} \right)^{3/2} \cdot \text{sign} \left(\tilde{u}_d \right) & |\tilde{u}_d| - 1 \geq 0 \\ 0 & |\tilde{u}_d| - 1 < 0 \end{cases},$$

$$\tilde{k}_2 = \frac{b_{\text{free}}^{1/2}}{\omega_d^2 m_d} k_2.$$

Hence, ζ_d is the damping ratio and $\tilde{k}_2$ displays the relative magnitude of the nonlinear with respect to the linear stiffness. The following parameter values are assigned throughout the studies, unless explicitly specified otherwise:

ζ_d	0.1
$\tilde{k}_2$	440

Fig. 4 shows the frequency response curve for the oscillator when subjected to single-harmonic excitation ($\tilde{F}(\tilde{t}) = \hat{F} \sin \omega t$). The displacement amplitude is normalized to the static response $|\tilde{u}_d|_{\omega=0}$, shown against the frequency ω divided by the natural frequency ω_0. The same figure shows the superimposed frequency response obtained by numerical time integration and that delivered by the PSA path-following technique.

The end stop is hit in the frequency bandwidth $0.93 \leq \omega/\omega_0 \leq 1.05$, where the response is saturated: the relative amplitude reaches a maximum around $|\tilde{u}_d|/|\tilde{u}_d|_{\omega=0} = 4.1$. The PSA path-following method displays a pronounced hardening branch for $1.05 \leq \omega/\omega_0 \leq 1.12$. This branch is partly found by the sequential path-following method in a forward sweep. The hardening branch is not captured by the harmonic balance, since this method iterates independently at each frequency towards a single stable solution. The contribution of the higher harmonics is revealed in Fig. 5, for $\omega/\omega_0 = 1.05$.

The dependence of the frequency response on the end stop stiffness is

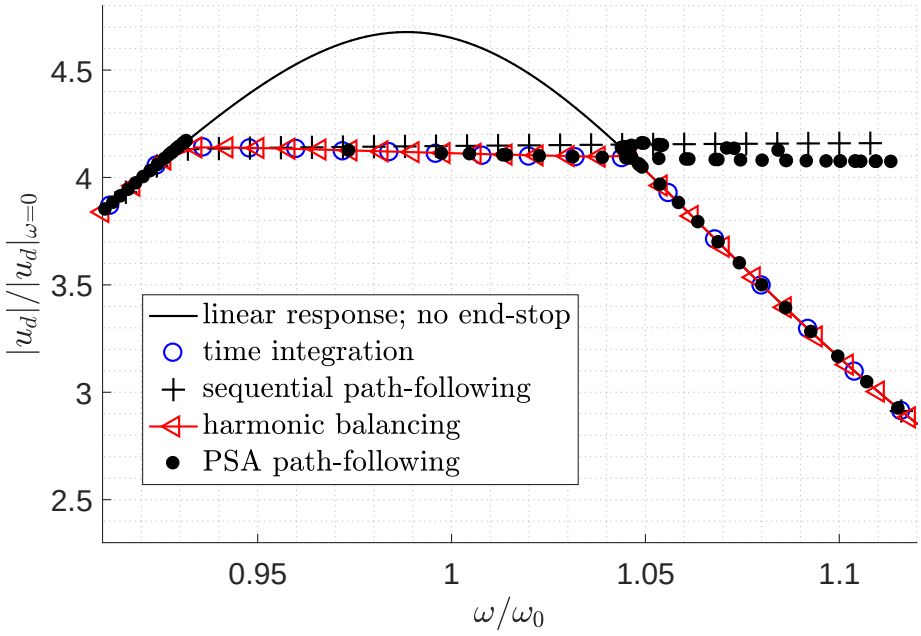

Figure 4: Frequency response for the single-dof oscillator with the end stop nonlinearity, subjected to single-harmonic excitation, zoomed in around the resonance. The PSA path-following algorithm [15] was borrowed and employed with permission.

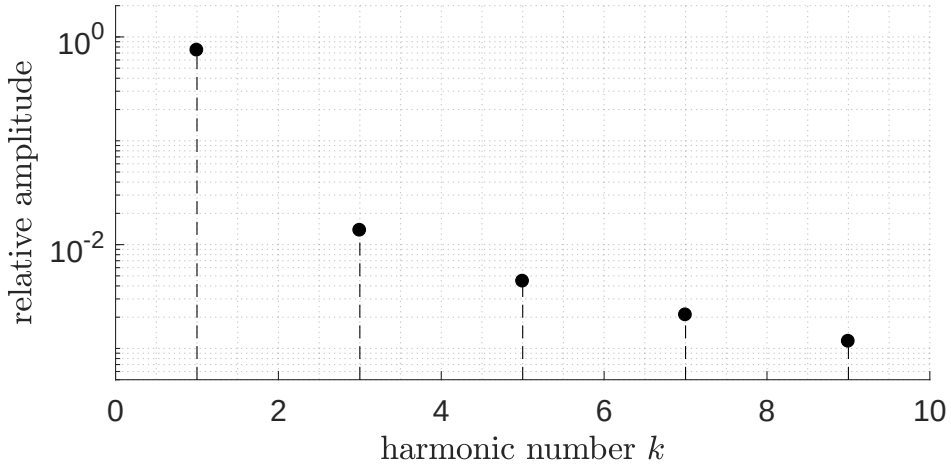

Figure 5: Harmonic components resulting from the AFT-HB method, for the single-dof oscillator with the end stop nonlinearity under single-harmonic excitation at $\omega = 1.05\omega_0$.

portrayed in Fig. 6. The AFT-HB method again shows a good agreement with the PSA path-following method, while tracing the stable parts ($0.93 \leq \omega/\omega_0 \leq 1.04$) of the nonlinear response. As the relative end stop stiffness is increased in the range $10 \leq \tilde{k}_2/\tilde{k}_d \leq 5 \cdot 10^2$ (where $\tilde{k}_d = 1$ due to the nondimensionalization), the response is increasingly more contained in the end stop region $0.93 \leq \omega/\omega_0 \leq 1.04$. For the upper bound value of $\tilde{k}_2/\tilde{k}_d = 5{\cdot}10^2$, the response level even decreases with increasing ω, as opposed to $\tilde{k}_2/\tilde{k}_d = 10$ and $\tilde{k}_2/\tilde{k}_d = 50$, for which the response level increases with increasing ω. This phenomenon can be interpreted as follows: the response amplitude can be seen as a multiplication of a static response and a dynamic amplification factor. The dynamic amplification factor depends on the damping ζ_d, while the static response amplitude depends on the stiffness. As ω is increased, the stiffness of the system increases due to the hardening effect (caused by $\tilde{k}_2$).

As a result, the total response amplitude relative to the linear case decreases for increasing ω.

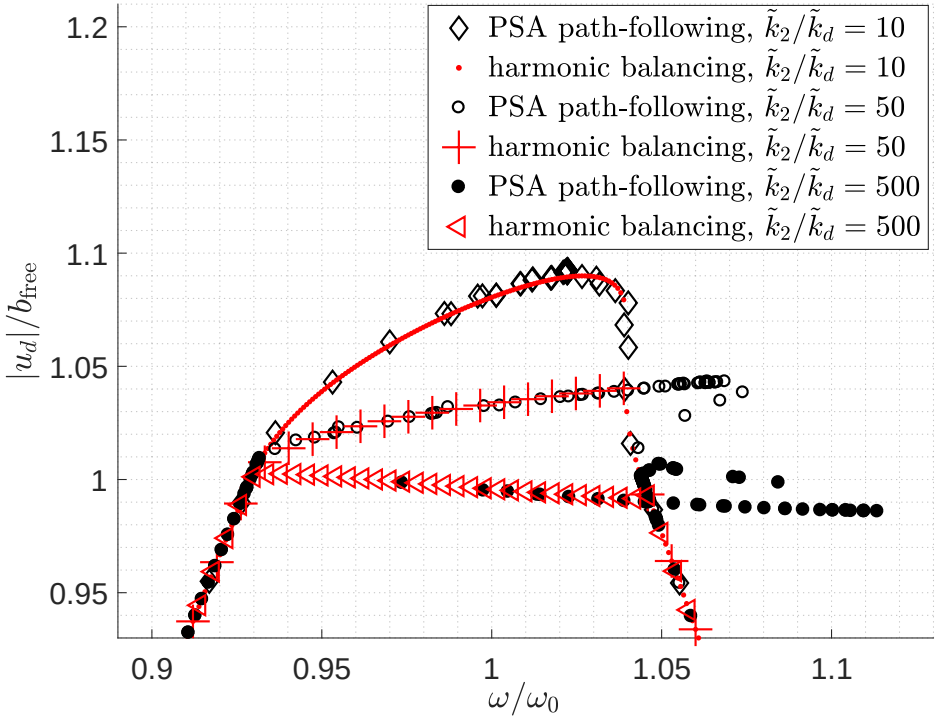

Figure 6: Frequency response of the single-dof oscillator with the end stop nonlinearity, under single-harmonic excitation, for different relative end stop stiffnesses. The AFT-HB method was carried out using 7 harmonics. The PSA path-following algorithm [15] was borrowed and employed with permission.

While a single-harmonic external excitation allows one to closely study the system response at each excitation frequency independently, realistic loads on structures such as seismic and hydrodynamic loads are multi-harmonic.

A multi-harmonic force vector with uniform distribution can be constructed

by summing a number of n_F harmonics:

$$\tilde{F}(t) = \frac{\hat{F}}{n_F} \sum_{i=1}^{n_F} \sin(\omega_i t + \phi_i), \tag{45}$$

where $\hat{F}$ is the excitation amplitude, which is constant so that all freqencies in the given spectrum exhibit the same force level; ϕ_i is a random phase, and there is no correlation between the phases from the different harmonics. In Fig. 7 a sample of this excitation vector is shown.

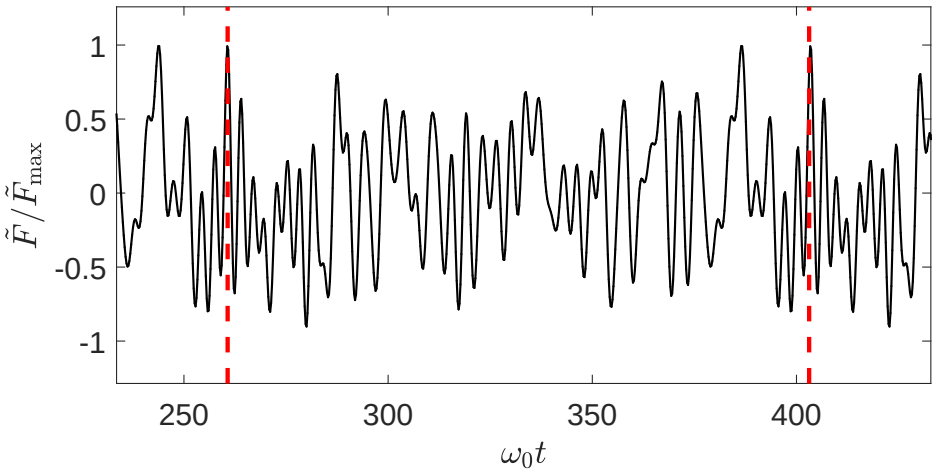

Figure 7: Time history of a multi-harmonic excitation as defined by Eq. 45. The period is signaled by the vertical dashed lines.

By introducing the force vector given by Eq. 45 in the nonlinear equation of motion (Eq. 7), containing $n_F = 100$ harmonic components, the time response is obtained and is shown in Fig. 8. The time history obtained with AFT-HB is in good agreement with time integration. Both methods show how the response is perturbed by the end stop at $\omega_0 t = 389$, and re-joins

the linear response between $410 \leq \omega_0 t \leq 420$. The FFT of the response is subsequently obtained after applying a Hanning window. The result is shown in Fig. 9.

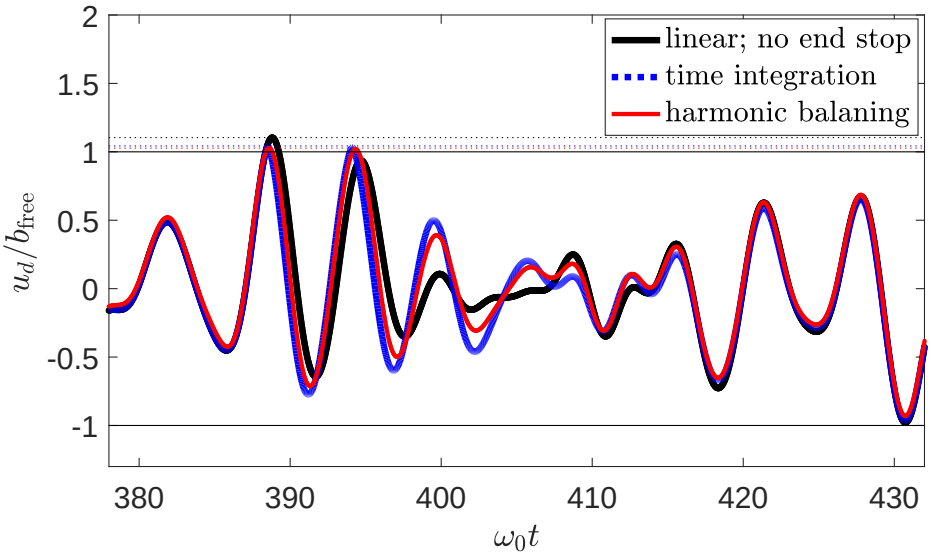

Figure 8: Time history of the relative displacement for the single-dof oscillator with end stop nonlinearity, under multi-harmonic excitation.

The apparent noisiness of the frequency response is a result of the randomness between phases in the excitation, causing a biased nonlinear response. By generating 130 realizations of the force vector (Eq. 45), by time integrating Eq. 7, hence obtaining different FFTs and, upon averaging, a smoother response is obtained and shown in Fig. 10. The response was also obtained via the AFT-HB method, as discussed in Sec. 3, by applying the forcing defined by Eq. 45 and assuming that the response contains the same harmonics. The response obtained via AFT-HB shows good agreement with the results obtained via time integration.

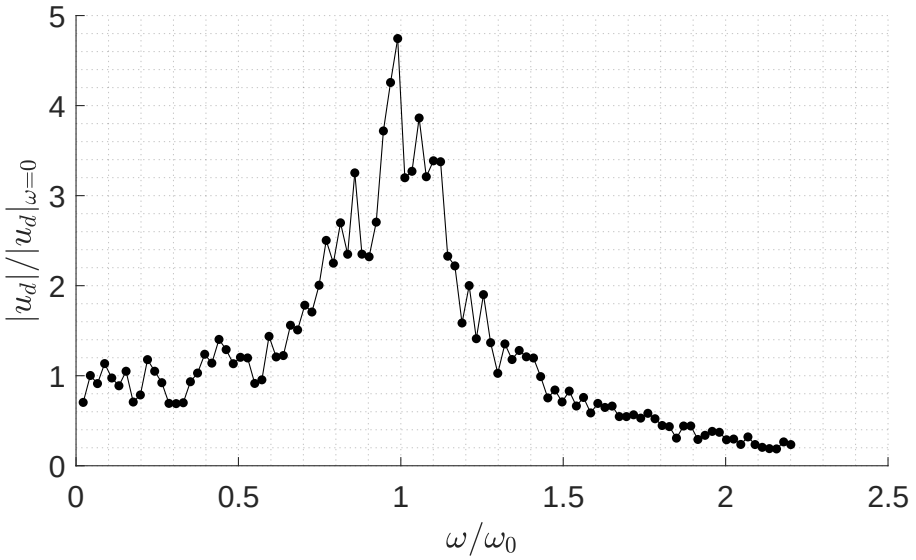

Figure 9: Frequency response of the single-dof oscillator with the end stop nonlinearity, under multi-harmonic excitation containing $n_F = 100$ harmonic components with uncorrelated phases.

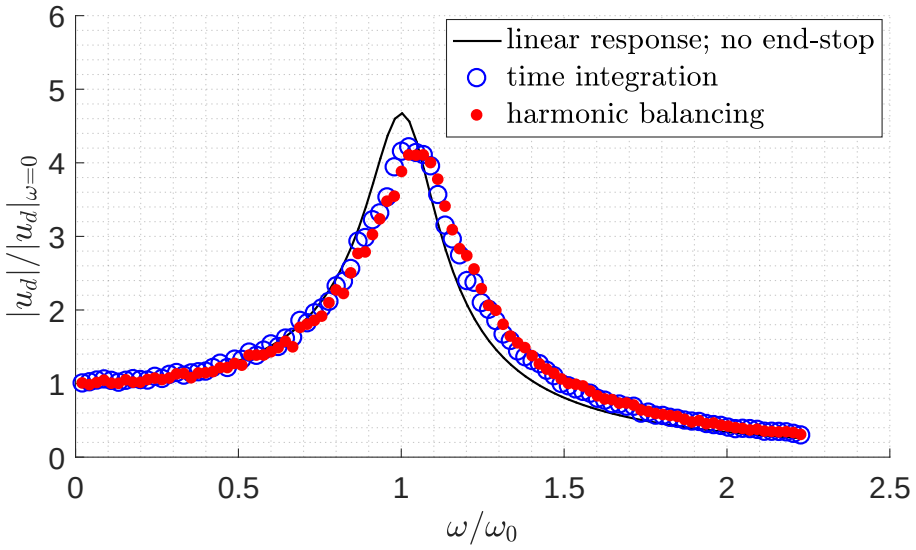

Figure 10: Average frequency response (taken from 130 individual responses) of the single-dof oscillator with the end stop nonlinearity, under multi-harmonic excitation containing $n_F = 100$ harmonic components with uncorrelated phases.

In contrast to the response to single-harmonic excitation (Fig. 4), no threshold behavior of the end stop is apparent in the averaged frequency response in Fig. 10. Due to the random phase relationship between the harmonics in the excitation, the values of ω at which the end stop is hit exhibit a probability distribution rather than a sharp transition. A smooth lowering of the amplitude, as well as a slight hardening can be observed in Fig. 10. Just as with the response amplitude reduction, this hardening is of smooth nature as opposed to the hardening branches corresponding to the single-harmonic external excitation, as was observed in Fig. 4.

4.2. Two-dof oscillator

After the performance of AFT-HB is studied for the single-dof oscillator, the proposed solution methodology is applied to the two-dof oscillator representing a structure with an attached TMD, where the TMD motion is limited by end stops, as is shown in Fig. 1. Following the same procedure as with the single-dof oscillator obtaining Eq. 43, the nondimensional equations of motion are derived for the two-dof oscillator (where $\omega_d = \sqrt{k_d/m_d}$ and $\omega_s = \sqrt{k_s/m_s}$):

$$\begin{bmatrix} 1 & 0 \\ 0 & \mu_s \end{bmatrix} \begin{bmatrix} \ddot{\tilde{u}}_d \\ \ddot{\tilde{u}}_s \end{bmatrix} + 2 \begin{bmatrix} \zeta_d & -\zeta_d \\ -\zeta_d & \alpha_s \mu_s \zeta_s + \zeta_d \end{bmatrix} \begin{bmatrix} \dot{\tilde{u}}_d \\ \dot{\tilde{u}}_s \end{bmatrix} + \begin{bmatrix} 1 & -1 \\ -1 & \alpha_s^2 \mu_s + 1 \end{bmatrix} \begin{bmatrix} \tilde{u}_d \\ \tilde{u}_s \end{bmatrix} + \begin{bmatrix} \tilde{f}^{\mathrm{NL}}(\tilde{u}) \\ 0 \end{bmatrix} = \begin{bmatrix} \tilde{F} \\ 0 \end{bmatrix}, \tag{46}$$

where:

$$\tilde{u}_s = u_s / b_{\text{free}} \tag{47}$$

$$\tilde{u} = \tilde{u}_d - \tilde{u}_s \tag{48}$$

$$\mu_s = \frac{m_s}{m_d}, \tag{49}$$

$$\alpha_s = \frac{\omega_s}{\omega_d}, \tag{50}$$

$$\tilde{F} = \frac{F}{m_d \omega_d^2 b_{\text{free}}}, \tag{51}$$

and:

$$\begin{aligned} \zeta_d &= \frac{c_d}{2 m_d \omega_d} \\ \zeta_s &= \frac{c_s}{2 m_s \omega_s} \\ \tilde{f}^{\text{NL}}(\tilde{u}) &= \end{aligned} \tag{52}$$

$$\begin{cases} \tilde{k}_2 \left(|\tilde{u}| - b_{\text{free}} \right)^{3/2} \cdot \text{sign}\left(\tilde{u}\right) & |\tilde{u}| - 1 \geq 0 \\ 0 & |\tilde{u}| - 1 < 0 \end{cases},$$

$$\tilde{k}_2 = \frac{b_{\text{free}}^{1/2}}{\omega_d^2 m_d} k_2.$$

The parameter values were chosen as follows:

μ_s	56
α_s	1.03
ζ_d	0.1 (same as in Sec. 4.1)
ζ_s	0.01
$\tilde{k}_2$	440 (same as in Sec. 4.1)

In Fig. 11 the frequency response is shown (zoomed in around the resonance), both for the structure displacement, as well as the relative TMD displacement, and the response of the stand alone structure.

From the relative TMD displacement shown in Fig. 11 one can observe that the end stop is hit in the frequency range $0.96 < \omega/\omega_0 < 1.03$, where the response of the configuration with the end stop deviates from the configuration without the end stop (the linear response). For the same frequency range, the structure displacement shows a deviation from the linear response, as expected. As a reference, the linear response of the structure with no TMD is also shown, to illustrate the resemblance with the response of the configuration structure with TMD with active end stop. The most obvious difference between these responses is a shift of eigenfrequency of about $0.005\omega/\omega_0$, which is explained by the difference in total mass when or when not including a TMD.

Similar to the single-dof oscillator with the end stop, the response curves show a threshold behavior; they deviate from the linear case for $|\tilde{u}| \geq 1$. As with the single-dof examples, the sequential path-following (forward Newton-Raphson iterations) overshoots the displacement with respect to the results from time domain simulations, although the values for ω at which the curves start deviating from the linear reference curve seem to coincide for both methods.

Around resonance ($\omega = \omega_0$), the time-integration method reveals a sharp increase in the relative TMD response. Time simulations are shown in Fig. 12, and reveal an asymmetric response according to the time-simulations (the DC component is $\tilde{u} = -0.4$). In an attempt to trace this behavior with

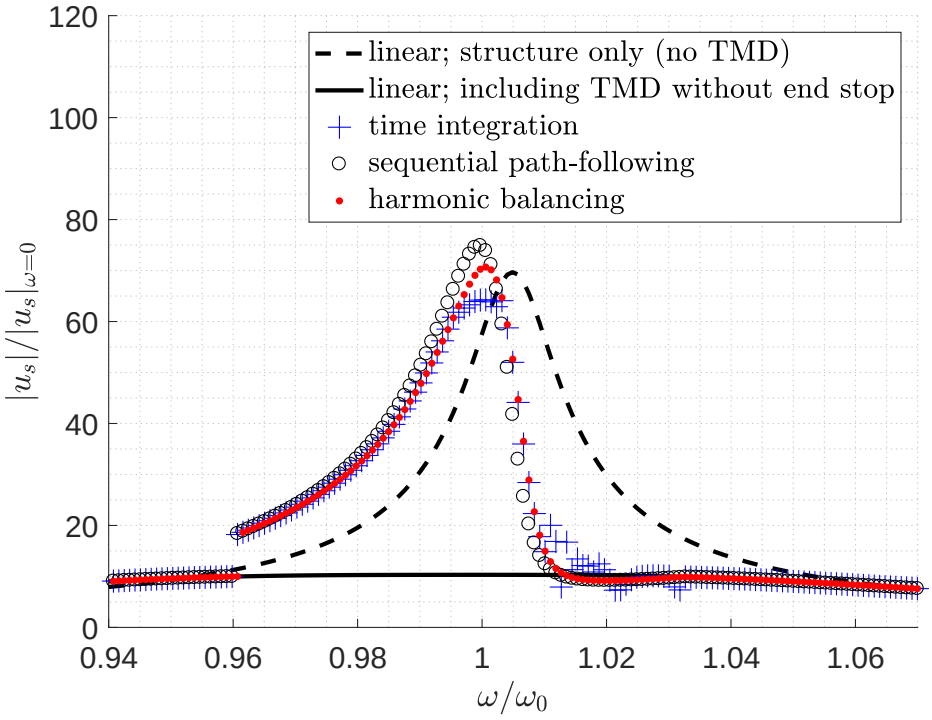

(a)

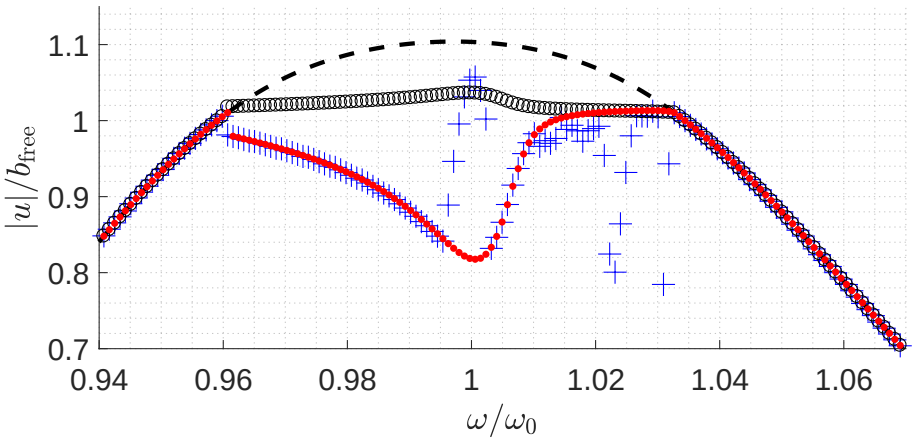

(b)

Figure 11: Frequency response of (a) structure displacement and (b) relative TMD displacement, for the two-dof damped structure with the end stop nonlinearity, subjected to single-harmonic excitation.

the AFT-HB method, the number of harmonic components was increased to around 50 (including DC terms), but the method was not able to yield this particular asymmetric branch of the solution.

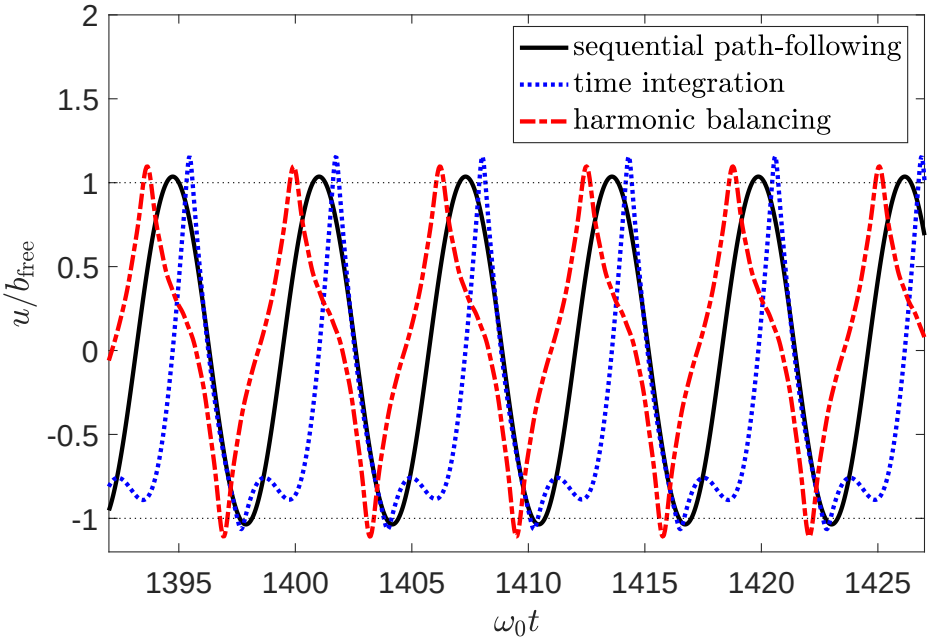

Figure 12: Time history of the relative TMD displacement for the two-dof oscillator with and without the end stop nonlinearity, under single-harmonic excitation at $\omega = \omega_0$.

Around $\omega/\omega_0 = 1.01$ the amplitude response of the structure drops to values slightly below the linear curve. Especially the time-integration method shows erratic behavior in the relative TMD displacment. Fig. 13 shows the time response of the relative TMD displacement. The behavior seems a 'beating' effect, where the difference between ω_0 and ω appears as a dominant frequency component in the displacement response. This frequency $\omega - \omega_0$ is

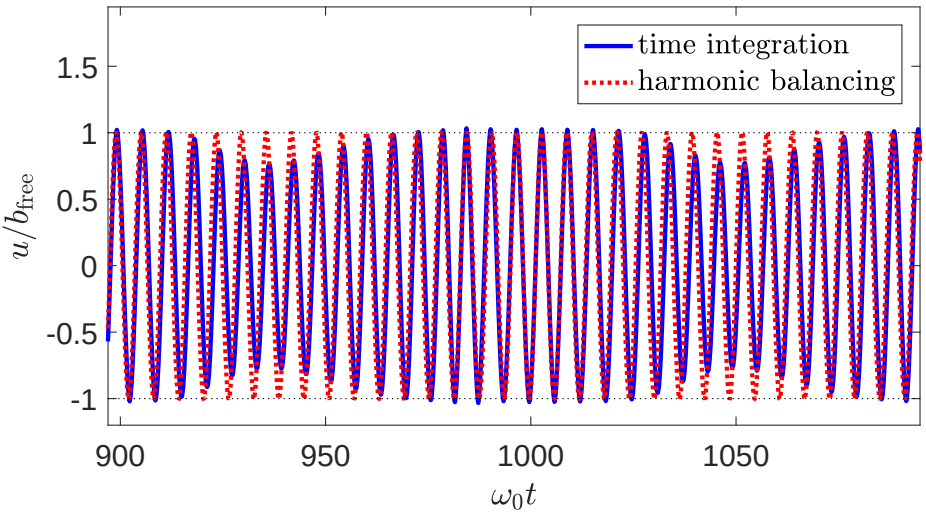

Figure 13: Time history of the relative TMD displacement for the two-dof oscillator with and without the end stop nonlinearity, under single-harmonic excitation at $\omega = 1.03\omega_0$.

far lower than the excitation frequencies ω, and is hence not caught by the AFT-HB method (since the lowest frequency in the response is ω), nor the sequential path-following method.

The two-dof structure with TMD is also studied for the case of multi-harmonic excitation, where the excitation is defined by Eq. 45. Following the same procedure described in Sec. 4.1, individual responses are obtained resulting from different multi-harmonic excitations, each containing 250 harmonics and random phases. The result is shown in Fig. 14.

Similar to the response for the single-dof oscillator shown in Fig. 10, the frequency response is of completely different nature than that under single-harmonic excitation (Fig. 11). Instead of a sharp transition towards a degradation of the TMD performance, a much milder effect is portrayed.

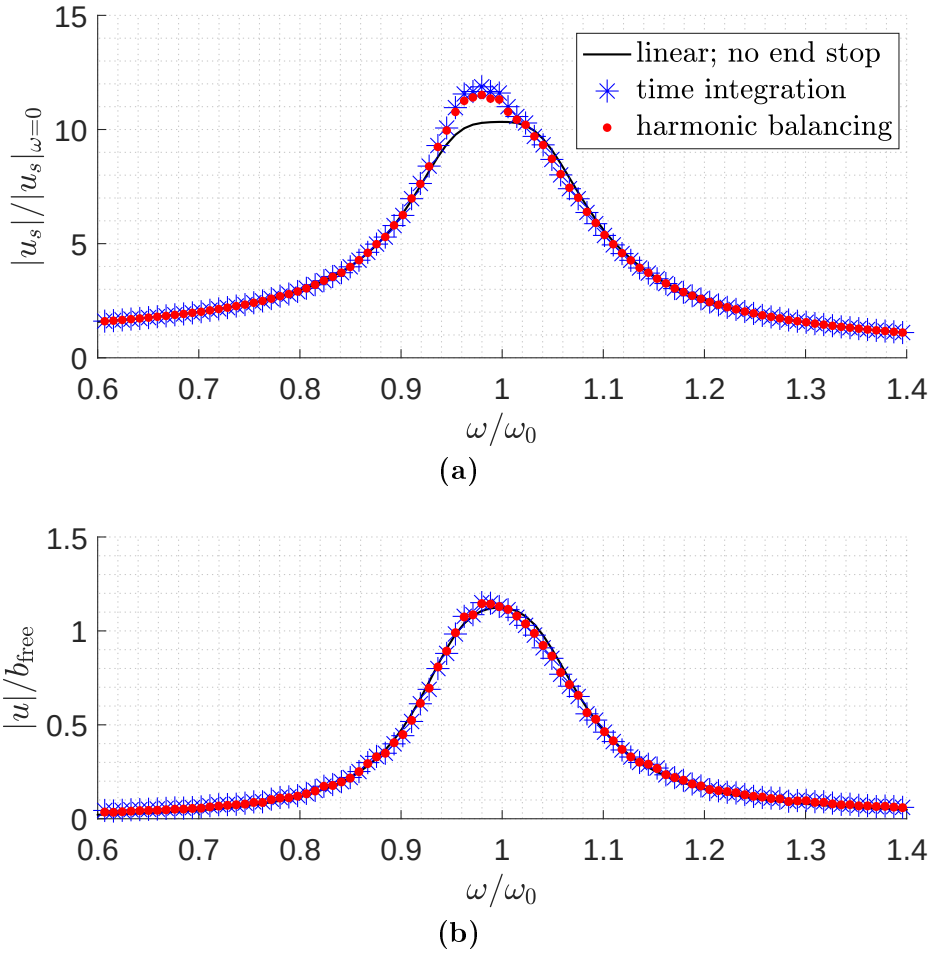

Figure 14: Average frequency response for (a) structure displacement and (b) relative TMD displacement, averaged over 150 individual responses, for the two-dof oscillator with the end stop nonlinearity, under multi-harmonic excitation containing $n_F = 250$ harmonic components with uncorrelated phases.

In the frequency band $0.9 \leq \omega/\omega_0 \leq 1.2$ the response of the TMD mass is slighly perturbed with respect to the linear case, causing a relative increase of the structure response of the order of 20%.

In Fig. 15 the time response is shown, for an individual response resulting from a multi-harmonic excitation defined in Eq. 45. Again, good agreement is shown between the AFT-HB method and time integration.

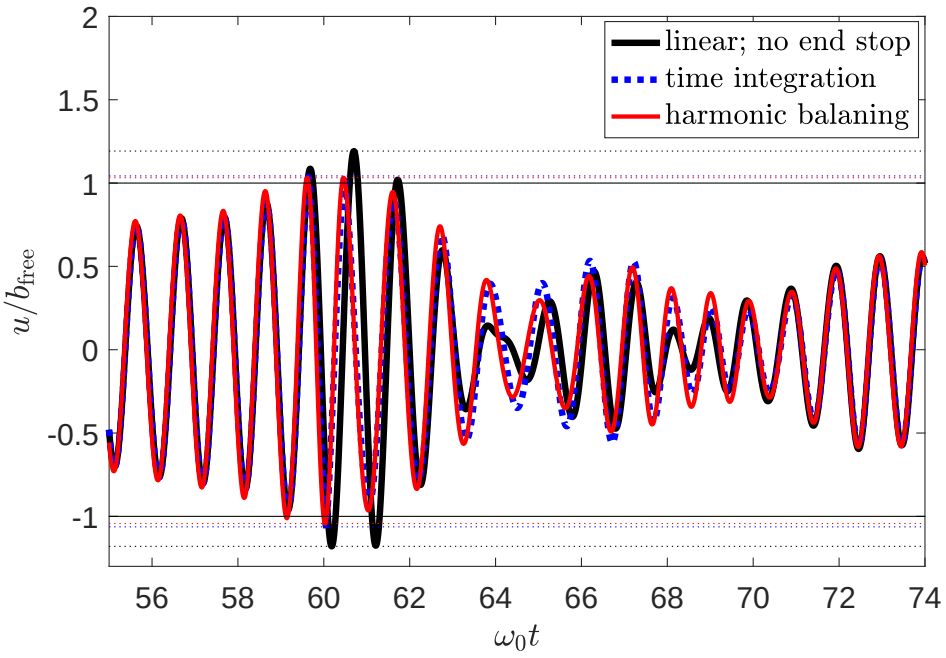

Figure 15: Time history of the relative TMD displacement for the two-dof oscillator with and without the end stop nonlinearity, under multi-harmonic excitation.

5. Conclusions

This work has proven that the AFT-HB is successful in solving nonsmooth problems involving hundreds of harmonic components in the excitation, hereby offering an alternative to conventional time integration solution methods. Two case studies were investigated: a single-dof oscillator with an end-stop nonlinearity, under an excitation including 100 harmonic components, and a two-dof oscillator with the same nonlinearity, under an excitation carrying 250 harmonics. The existing scope of the AFT-HB method is extended by incorporating many harmonic excitations. Moreover, insights were gained on the nature of the system response under such loads.

All modeling results were verified by a Newmark time integration method. The results for single harmonic excitations were further verified by employing a PSA path-following procedure [15].

The frequency response of the mass-spring-damper system with an end stop nonlinearity was shown to depend very much on the type of excitation. Two extreme scenarios were considered: single-harmonic and multi-harmonic excitations, the amplitude of which was uniformly distributed over the range of frequencies. The end stop was found to saturate the response of both single- and two-dof systems under single harmonic excitation, thus suggesting a severe degradation in the performance of the represented TMD when attached to a structure as discussed in Sec. 4.2.

For multi-harmonic excitations with random phase relationship, this performance degradation was found to be much milder and less binary, due to the stochastic nature of the excitation.

References

[1] I. D. Aiken, J. M. Kelly, Comparative study of four passive energy dissipation systems, NZ National Society of Earthquake Engineering Bulletin. 25 (1992) 175–192.

[2] T. T. Soong, B. F. SpencerJr, Supplemental energy dissipation: state-of-the-art and state-of-the-practice, Engineering Structures. 24 (2002) 243–259.

[3] M. C. Constantinou, M. D. Symans, Experimental study of seismic response of buildings with supplemental fluid dampers, The Structural Design of Tall and Special Buildings. 2 (1993) 93–132.

[4] G. Stewart, M. Lackner, Offshore wind turbine load reduction employing optimal passive tuned mass damping systems, IEEE transactions on Control Systems Technology. 21 (2013) 1090–1104.

[5] L. L. Chung, L. Y. Wu, H. H. Huang, C. H. Chang, K. H. Lien, Optimal design theories of tuned mass dampers with nonlinear viscous damping, Earthquake Engineering and Engineering Vibration. 8 (2009) 547–560.

[6] C. Sun, S. Nagarajaiah, A. J. Dick, Experimental investigation of vibration attenuation using nonlinear tuned mass damper and pendulum tuned mass damper in parallel, Nonlinear Dynamics. 78 (4) (2014) 2699–2715.

[7] N. Carpineto, W. Lacarbonara, F. Vestroni, Hysteretic tuned mass dampers for structural vibration mitigation, Journal of Sound and Vibration. 333 (2013) 1302–1318.

[8] A. Casalotti, W. Lacarbonara, A. Arena, Mitigation of post-flutter oscillations in suspension bridges by hysteretic tuned mass dampers, Engineering Structures. 69 (2014) 62–71.

[9] B. Carboni, W. Lacarbonara, Nonlinear dynamic response of a new hysteretic rheological device: experiments and computations, Nonlinear Dynamics. 83 (2016) 23–39.

[10] B. Carboni, W. Lacarbonara, A nonlinear vibration absorber with pinched hysteresis: theory and experiments, Journal of Engineering Mechanics. 142 (5) (2016) 23.

[11] A. Casalotti, W. Lacarbonara, Tailoring of pinched hysteresis for nonlinear vibration absorption via asymptotic analysis, International Journal of Non-Linear Mechanics. 94 (2017) 59–71.

[12] A. Casalotti, S. El-Borgi, W. Lacarbonara, Metamaterial beam with embedded nonlinear vibration absorbers, Journal of Non-Linear Mechanics. 98 (2018) 32–42.

[13] A. H. Nayfeh, Introduction to Perturbation Techniques, Wiley, Blacksburg, Virginia, 1993.

[14] W. Lacarbonara, Nonlinear Structural Mechanics: Theory, Dynamical Phenomena and Modeling., Springer, New York, 2013, iSBN 978-1-4419-1276-3.

[15] W. Lacarbonara, B. Carboni, A Matlab pseudo-arclength path-following software for smooth and nonsmooth dynamical systems, Sapienza University of Rome, 2013.

[16] H. Xiong, X. Kong, H. Li, Z. Yang, Vibration analysis of nonlinear systems with the bilinear hysteretic oscillator by incremental harmonic balance method, Communications in Nonlinear Science and Numerical Simulation. 42 (2017) 437–450.

[17] Z. Zhang, Y. Chen, Harmonic balance method with alternating frequency/time domain technique for nonlinear dynamical system with fractional exponential, Applied Mathematics and Mechanics. 35 (2014) 423–436.

[18] C. Pierre, A. A. Ferri, E. H. Dowell, Multi-harmonic analysis of dry friction damped systems using and incremental harmonic balance method, Journal of Applied Mechanics. 52 (1985) 958–964.

[19] M. Guskov, J. J. Sinou, F. Thouverez, Multi-dimensional harmonic balance applied to rotor dynamics, Mechanics Research Communications. 35 (2008) 537–545.

[20] R. Jankowski, Analytical expression between the impact damping ratio and the coefficient of restitution in the non-linear viscoelastic model of structural pounding, Earthquake Engineering & Structural Dynamics. 35 (2006) 517–524.

[21] H. S. Jing, M. Young, Impact interactions between two vibration systems under random excitation, Earthquake Engineering & Structural Dynamics. 20 (1991) 667–681.

[22] M. Papadrakakis, H. Mouzakis, N. Plevris, S. Bitzarakis, A lagrange

multiplier solution method for pounding of buildings during earthquakes, Earthquake Engineering and Structural Dynamics. 20 (1991) 981–998.

[23] A. H. Nayfeh, D. T. Mook, Nonlinear Oscillations, Wiley-Interscience, New York, 1979.

[24] G. von Groll, D. J. Ewins, The harmonic balance method with arc-length continuation in rotor/stator contact problems, Vol. 241, Journal of Sound and Vibration., 2001.